CHIN. PHYS. LETT. Vol. 38, No. 2 (2021) 023201

Multiple Auger Decay Following Xe^+ $(4p_{3/2}^{-1})$ Ionization

Zhenqi Liu(刘振旗)[1], Qing Liu(刘青)[1], Yulong Ma(马玉龙)[2], Fuyang Zhou(周福阳)[3], and Yizhi Qu(屈一至)[1*]

[1]*School of Optoelectronics, University of Chinese Academy of Sciences, Beijing 100049, China*
[2]*College of Physics and Electronic Engineering, Northwest Normal University, Lanzhou 730070, China*
[3]*Data Center for High Energy Density Physics, Institute of Applied Physics and Computational Mathematics, Beijing 100088, China*

(Received 4 October 2020; accepted 18 November 2020; published online 27 January 2021)

The Auger decay for the many-electron Xe^+ $(4p_{3/2}^{-1})$ state is studied in detail, using multistep approaches. It is found that the single Auger decay channels are primarily Coster–Kronig processes, which is in accord with other theoretical and experimental results. The double and triple Auger decays result primarily from cascade processes, i.e., the sequential two-step and three-step Auger decay, and as such, the contributions from direct processes can be neglected. Level-to-level rates for single, double, and triple decays are obtained, based on which comprehensive Auger electron spectra and ion yields are obtained. Our decay paths and Auger electron spectra are in agreement with the experimental analysis [Hikosaka *et al.*, Phys. Rev. A 76 (2007) 032708], and our ion yield ratios (Xe^{2+}: Xe^{3+}: Xe^{4+} = 4.6 : 87.0 : 8.4) are also in line with their values (5.0 : 86.0 : 9.0). However, with respect to the ion yield ratios, a discrepancy still remains among the experimental and theoretical results. Taking into account the complexity of Xe's electronic structure, further, more detailed experiments are still required.

DOI: 10.1088/0256-307X/38/2/023201

The multiple Auger (MA) decay of a core-ionized state produced by photon, electron, or ion impact, can proceed with emissions of two, three, or more Auger electrons.[1–7] This has aroused the interest of both theoretical and experimental research teams for some time.[4,8,9] The study of MA processes contribute to a better understanding of the electronic structure and the electron dynamics underlying high-charge-state and hollow atoms.[2,10] The MA spectroscopy from emitted (Auger) electrons with characteristic energies represents a powerful tool for investigating electron correlation effects and many-body problems in atomic processes.[11]

The independent particle model (frozen atomic structure approximation)[8] fails to describe MA for high-order processes, which are usually studied in the context of many-body perturbation theory (MBPT).[8] To date, many theoretical works have been published based on MBPT to study the MA processes of simple atomic systems, with good results.[12–15] In contrast, for heavier elements with complex atomic structures, such as Xe, great challenges still remain. For example, in the case of Xe^+ $(4p^{-1})$, the one-electron picture completely breaks down in the face of anomalous photoelectron peak structures found via experimental observation:[6,16–22] the expected $4p_{1/2}$ photoelectron line is dissolved and invisible, while the $4p_{3/2}$ structure consists of several fine components, due to the strong interaction with $4d^{-2}nf$.[6,16–24] With respect to the experimental measurements of Eland *et al.*,[6] Hikosaka *et al.*[19] and Hayaishi *et al.*[22] in relation to Xe^+ $(4p_{3/2}^{-1})$ MA decay, all observed the ion yields of Xe^{2+}, Xe^{3+} and Xe^{4+} produced by single Auger (SA), double Auger (DA), and triple Auger (TA). Of the above research teams, Hikosaka *et al.*[19] investigated the decay process most comprehensively; they further measured SA, DA and TA decay electron spectra, and provided detailed analysis.

Although previous theoretical research has been undertaken with regard to the Auger decay of Xe^+ $(4p_{3/2}^{-1})$ states,[18,24] to the best of our knowledge, a detailed numerical simulation of the overall two-step and three-step Auger cascades, in order to study the electron correlations and to obtain Auger electron spectra with satisfactory accuracy, has yet to be attempted. In this Letter, we present a theoretical study of the SA, DA and TA decays of Xe^+ $(4p_{3/2}^{-1})$ within the framework of MBPT, including all important Auger decays between fine-structure levels, in order to obtain detailed Auger electron spectra and ion yields, and compare them with other theoretical and experimental data.[6,18,19,22,24]

As a basis for discussion, and to highlight possible decay channels, the energy levels of Xe^+, Xe^{2+}, Xe^{3+} and Xe^{4+} ions relative to the ground level of the Xe atom are displayed in Fig. 1. Here, SA, DA and TA decays of Xe^+ $(4p_{3/2}^{-1})$ are possible, since such core-ionized states are energetically above the ionization threshold of the Xe^{2+}, Xe^{3+} and Xe^{4+} ions.

Supported by the National Key Research and Development Program of China (Grant No. 2017YFA0402300), and the National Natural Science Foundation of China (Grant Nos. 11774344 and 11474033).
*Corresponding author. Email: yzqu@ucas.edu.cn
© 2021 Chinese Physical Society and IOP Publishing Ltd

The SA decay includes Coster–Kronig (C-K)[25] decay, whereby a higher subshell with the same shell as the initial state hole fills that hole (e.g., $4p \to 4d$) and normal decay, whereby a valence electron ($5s$ or $5p$) fills the $4p$ hole with the ionization of another valence electron, i.e., only the valence electrons take part in the decay process. Generally, two different and competing direct and cascade[8] mechanisms can be distinguished. The emission of many electrons can be simultaneous in the direct MA, whereas it can proceed in a stepwise manner through the creation and decay of an intermediate autoionizing state in the cascade process. For lighter atomic systems, such as C^+ $(1s^{-1})$[5,26] and Ne^+ $(1s^{-1})$,[14] the contributions of direct processes are too important to be neglected.[8] However, with respect to the DA and TA decays of Xe^+ $(4p_{3/2}^{-1})$, cascade processes are dominant.[19] This is because $4d^{-1}V^{-1}$ (V represents valence orbitals $5s$ and $5p$) and $4d^{-1}V^{-2}nl$ ($nl \neq 5s$ and $5p$) in Xe^{2+} are readily formed by C-K decay; moreover, such $4d$-hole states, lying above the ionization thresholds of Xe^{3+} and Xe^{4+} ions (see Fig. 1), will decay further via the emission of one and two electrons, leading to the cascade DA and TA processes, respectively. On the other hand, according to our test calculations, the contribution of direct processes is smaller than that of cascade processes by at least two orders of magnitude. Therefore, only the cascade processes for DA and TA decay are considered in this study.

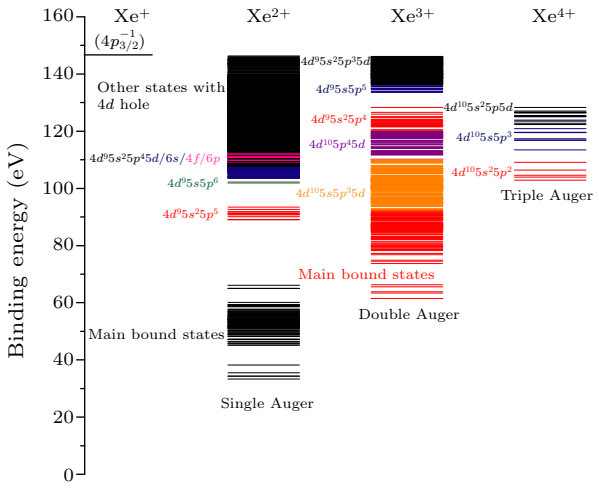

Fig. 1. Energy levels of Xe^+, Xe^{2+}, $Xe^{3+}$and Xe^{4+} ions, relative to the ground level of the Xe atom. Here, Xe^+ $(4p_{3/2}^{-1})$ and main configurations, including single, double and triple Auger are presented.

In the lowest order of perturbation theory, the SA rate can be obtained by[10,27,28]

$$A^1_{\alpha\beta} = 2\left|\left\langle \psi^+_\beta, \kappa; J_T M_T \right| \sum_{i<j}^{N} \frac{1}{r_{ij}} \left|\psi_\alpha\right\rangle\right|^2, \tag{1}$$

where $|\psi_\alpha\rangle$ represents the initial autoionizing state, and $|\psi^+_\beta, \kappa; J_T M_T\rangle M_T$ is the final ionic state $|\psi^+_\beta\rangle$ plus a continuum Auger electron with the relativistic angular quantum number κ; J_T and M_T denote the total angular momentum and the magnetic quantum number of the final ionic state, respectively. In order to obtain the SA rates, the XAUGER component of the RATIP program[29] was performed, in which the continuum orbitals for the Auger electrons are generated as distorted waves in the potential of final ionic states. Further details may be found in Ref. [29].

In the cascade DA process, the initial state Xe^+ $(4p_{3/2}^{-1})$ primarily decays to intermediate states of Xe^{2+} ions, which embed energetically within the continuum of the states of the Xe^{3+} ion, and will decay further via SA decay. The corresponding rate can be obtained from the expression[8,12–15]

$$A^{DA}_{if} = \sum_m A^{SA}_{im} \frac{A^{SA}_{mf}}{\Gamma_m}, \tag{2}$$

where A^{SA}_{im} and A^{SA}_{mf} denote the SA rates from the initial state Xe^+ $(4p_{3/2}^{-1})$ to the intermediate autoionizing state, m and then decay to the final state, f; Γ_m is the total width of the intermediate state, m. In addition, only the Auger rates are employed to determine the width, based on the fact that radiative decay rates are typically suppressed by several orders of magnitude for whichever autoionizing state is involved.

With respect to the cascade TA process, the third Auger electron is emitted for those states of the Xe^{3+} ion formed by the cascade DA process given in Eq. (2), which lies above the ionization threshold of the Xe^{4+} ion. Thus, the cascade TA rate is given by

$$A^{TA}_{if} = \sum_m A^{SA}_{im} \sum_n \frac{A^{SA}_{mn}}{\Gamma_m} \frac{A^{SA}_{nf}}{\Gamma_n}, \tag{3}$$

where A^{SA}_{nf} is the SA rate of the intermediate state, n (with the total width Γ_n), of Xe^{3+} ions produced by the cascade DA to the final states of the Xe^{4+} ion.

In this work, the GRASP2K[30–32] program was employed to generate all bound-state wave functions, based on the multiconfiguration Dirac–Fock (MCDF) method.[33] Using this method, one can optimize the single-electron orbitals and atomic state functions (ASFs) via self-consistency procedures, accompanied by collating all configuration state functions interacting with ASFs to include the electron correlation. Therefore, the following configurations are included for the initial states Xe^+ $(4p_{3/2}^{-1})$, Xe^{2+}, Xe^{3+}, and Xe^{4+} in this study:

(I) Xe^+ $(4p_{3/2}^{-1})$: $4p^5 4d^{10} 5s^2 5p^6$, $4p^6 4d^8 5s^2 5p^6 4f$, $4p^6 4d^8 5s^2 5p^6 6p$, $4p^5 4d^{10}[5s, 5p]^7 nl$,

(Ⅱ) Xe^{2+}: $4p^6 4d^{10}[5s, 5p]^6$, $4p^6 4d^9[5s, 5p]^7$, $4p^6 4d^{10}[5s, 5p]^5 nl$, $4p^6 4d^9[5s, 5p]^6 nl$,

(Ⅲ) Xe^{3+}: $4p^6 4d^{10}[5s, 5p]^5$, $4p^6 4d^9[5s, 5p]^6$, $4p^6 4d^{10}[5s, 5p]^4 nl$, $4p^6 4d^9[5s, 5p]^5 nl$,

(Ⅳ) Xe^{4+}: $4p^6 4d^{10}[5s,5p]^4$,$4p^6 4d^{10}[5s,5p]^3 nl$. Here $[5s,5p]^m$ indicates that m electrons are distributed between the $5s$ and $5p$ orbitals, and $nl = 4f$, $5d$, $5f$, $6s$, $6p$, $6d$, $7s$ and $7p$. Note that nonorthogonal orbital functions between initial and final states do not affect our results.[14,29,34–36]

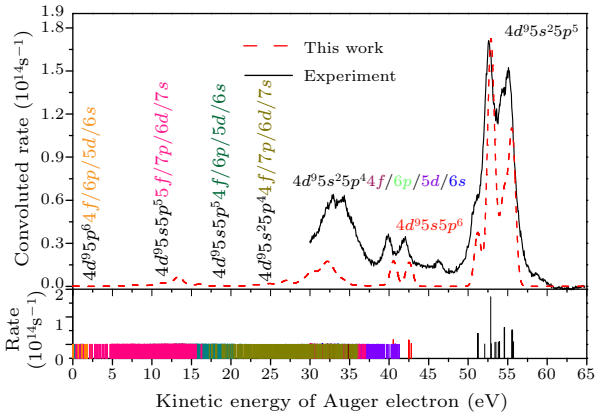

Fig. 2. Theoretical and experimental[19] Coster–Kronig SA spectra for Xe^+ $(4p_{3/2}^{-1})$ decay. The histogram with colors corresponds to different final-state transition rates.

In order to compare the experimental Auger electron spectra,[19] our theoretical Auger rates are convolved via a Gaussian profile of the full width at half maximum (FWHM) for a certain energy range of the Auger electron, based on the energy resolving power of the apparatus $E/\Delta E \approx 50$ in the experiment.[19] Figure 2 shows the electron spectra convolved using a Gaussian profile of 1 eV FWHM (on the basis of our spectra at 50 eV) and the experimental[19] results for the C-K decay. The possible transition rates are indicated by the histograms below Fig. 2, where the colors correspond to different main configurations of Xe^{2+}. In Fig. 2, the main peak around 55 eV, and the peaks around 43 eV and 35 eV, originate from the $4d^95s^25p^5$, $4d^95s5p^6$, and $4d^95s^25p^4nl$ ($nl = 4f$, $5d$, $6s$ and $6p$), respectively. The forbidden transitions of Xe^+ $(4p_{3/2}^{-1}) \rightarrow 4d^{-1}V^{-2}nl$ can only be attributed to the configuration interaction (CI). Therefore, the electron correlation effects in the Auger decay of Xe^+ $(4p_{3/2}^{-1})$ must be taken into consideration with caution. On the other hand, the intensities of those spectra below 50 eV are clearly below those achieved experimentally,[19] but we note that the background of the coincidences could contribute to the intensities of the SA electron spectra derived experimentally.[19] For normal SA transition, the spectra convolved with 2 eV FWHM in this work agree well with the experimental results,[19] as shown in Fig. 3. The main peak corresponds to the Xe^+ $(4p_{3/2}^{-1}) \rightarrow$ ground states $4d^{10}5s^25p^4$ with about 113 eV, on the right of the figure. The two small peaks on the left are generated by $4d^{10}5s5p^5$, $4d^{10}5s^25p^35d$, and $4d^{10}5s^25p^36s$ configurations. It is clear that the energy positions of the ground states are in better agreement with the experimental values than those for excited states.

As presented in Figs. 2 and 3, our C-K and normal SA decay spectra are all consistent with the experimental measurements.[19] For a more detailed comparison, the branching ratios (BRs) populating the main Xe^{2+} states are listed in Table 1, along with the theoretical[18,24] and experimental values.[19]

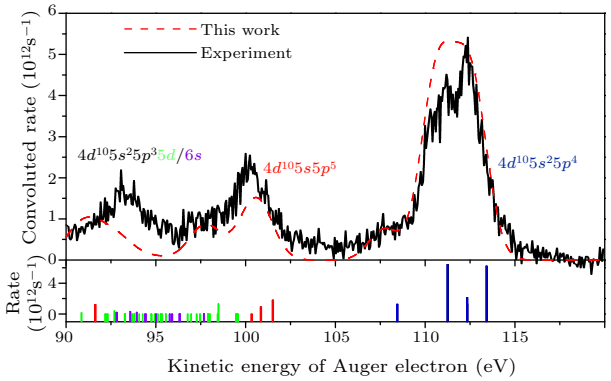

Fig. 3. Theoretical and experimental[19] normal SA decay spectra for Xe^+ $(4p_{3/2}^{-1})$ decay. The histogram with colors corresponds to different final-state transition rates.

Table 1. Branching ratios (BRs), including other theoretical and observed values for populating the main transition channels by SA decay.

Xe^{2+}		BR			
		This work	Theory[18]	Theory[24]	Experiment[19]
Coster–Kronig decay	$4d^95s^25p^5$	71.8	59.4	68.9	66.0
	$4d^95s5p^6$	5.9	8.3	27.4	6.0
	$4d^95s^25p^4$[$4f$, $6p$, $5d$ and $6s$]	11.0	25.3		17.0
	Other $4d$-hole states	6.7			6.0
	Total	95.4	93.0	96.3	95.0
Normal decay	$4d^{10}5s^25p^4$	2.9	4.8	2.5	3.0
	$4d^{10}5s5p^5$	0.7	1.0	1.2	1.0
	Other states	1.0[a]	1.2[b]		1.0[c]
	Total	4.6	7.0	3.7	5.0

[a]From all the other normal decay states in this work.
[b]From the $4d^{10}5s^25p^3$[$5d$ and $6s$].
[c]From the $4d^{10}5s5p^5$ at 92 eV Auger energy.

In Table 1, the contributions from the C-K transition dominate, accounting for 95.4% of the total BR in our work, which is in good agreement with the experimental BR of 95.0%[19] and theoretical ratios of 93.0%[18,19] and 96.3%.[24] The C-K decays preferentially into $4d^{-1}V^{-1}$, with a BR of 77.7% (71.8% for $4d^95s^25p^5$ and 5.9% for $4d^95s5p^6$) which agrees reasonably with both theoretical and experimental results of 67.7%[18,19] and 72.0%.[19] However, for the transition of Xe^+ $(4p_{3/2}^{-1}) \rightarrow Xe^{2+}4d^95s5p^6$, the BR 27.4% calculated by Kochur *et al.*[24] is much greater than ours and the other listed values.[18,19] A possible reason for this is that the number of configurations adopted by Kochur *et al.*[24] is too low, and that in consequence, some important correlation effects are not included, e.g., the populations of the $4d^{-1}V^{-2}nl$ states ($nl = 4f$, $5d$, $5f$, $6s$, $6p$, $6d$, $7s$ and $7p$) are missing from their calculations.[24] By contrast, in our calculations, the important configurations are included as much as possible. In Table 1, (i) our BR 5.9% for Xe^+ $(4p_{3/2}^{-1}) \rightarrow Xe^{2+}4d^95s5p^6$ agrees well with experimental values of 6.0%[19] and 8.3%;[18] (ii) the transition of the Xe^+ $(4p_{3/2}^{-1}) \rightarrow Xe^{2+}4d^{-1}V^{-2}nl$ are allowed, with a BR of 17.7% resulting from 11.0% for $4d^95s^25p^4nl$ ($nl = 4f$, $6p$, $5d$ and $6s$) and 6.7% for "other 4d-hole states" in our calculation, which is in agreement with the experimental and theoretical values of 23.0%[19] and 25.3%,[18] respectively. This once again emphasizes the importance of electron correlations with respect to the Auger decay of Xe^+ $(4p_{3/2}^{-1})$. Furthermore, Hikosaka *et al.*[19] obtained a detailed Auger electron spectrum, allowing them to identify the relative intensities of the transition Xe^+ $(4p_{3/2}^{-1}) \rightarrow Xe^{2+}4d^{-1}V^{-2}nl$, with the exception of $4d^95s^25p^4nl$ ($nl = 4f$, $6p$, $5d$ and $6s$), where most of this Xe^{2+} intermediate states will participate in the cascade TA processes, forming the Xe^{4+} ion. Based on our calculations, such intermediate states tend to originate from $4d^95s^25p^4nl$ ($nl = 5f$, $7p$, $6d$ and $7s$), $4d^95s5p^5nl$ ($nl = 4f$, $6p$, $5d$, $6s$, $5f$, $7p$, $6d$ and $7s$) and $4d^95p^6nl$ ($nl = 4f$, $6p$, $5d$ and $6s$) with a BR of 6.7%, which agrees well with the experimental value of 6.0%[19] given in Table 1.

Compared to the C-K transition above, normal SA decay makes only a small contribution to the total SA decay. In SA decay, the transition of Xe^+ $(4p_{3/2}^{-1}) \rightarrow Xe^{2+}4d^{10}5s^25p^4$ dominates, with a BR of 2.9%. The BR of Xe^+ $(4p_{3/2}^{-1}) \rightarrow$"other states" indicated in Table 1 is estimated to be 1.0%, which is in good agreement with the previous theoretical and experimental values of 1.2%[18] and 1.0%,[19] respectively, while the populations are missing in the calculations[24] due to absence of important configurations. In addition, our calculated BR of the weakest transition of Xe^+ $(4p_{3/2}^{-1}) \rightarrow Xe^{2+}4d^{10}5s5p^5$ is determined to be 0.7%, which is in reasonable agreement with the theoretical[18,24] and experimental values.[19]

The lifetime of Xe^+ $(4p_{3/2}^{-1})$ in this work is calculated as 0.39 eV, which is in good agreement with the measured value of 0.33 ± 0.03 eV in Ref. [17].

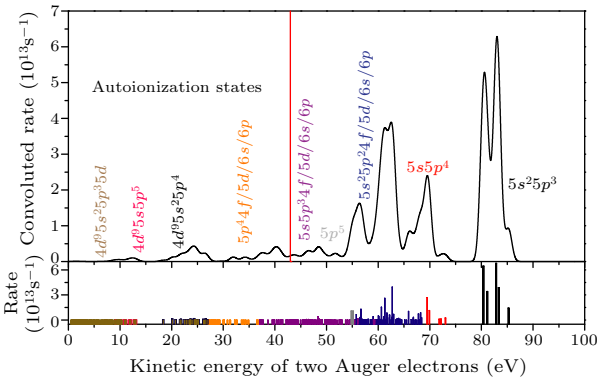

Fig. 4. Theoretical DA Auger spectra from Xe^+ $(4p_{3/2}^{-1})$ to Xe^{3+} are shifted 2 eV toward left (lower energy). The solid red line represents first ionization threshold of Xe^{3+} and the histogram with colors corresponds to different final-state transition rates.

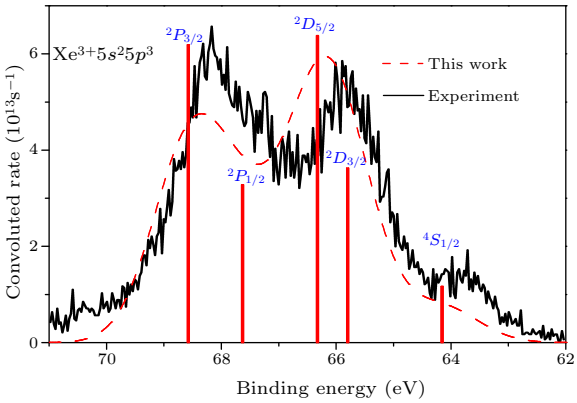

Fig. 5. Theoretical and experimental[19] Auger spectra from $Xe^{2+}4d^95s^25p^5$ to $Xe^{3+}4d^{10}5s^25p^3$. The red verticals are our transition rates.

As shown in Fig. 1, the energy levels of C-K Xe^{2+} final states are above the ground state of Xe^{3+}, which will decay via a DA process. Our electron spectra for the DA decay into Xe^{3+} are displayed in Fig. 4, with 2 eV shifted toward lower energy to match the experimental spectra, and convolved with a Gaussian profile of 1.5 eV FWHM. The correlation energy always remains; in our calculation with limited ASFs, the correlation energy is variant for each ionic state, so the theoretical energy difference may differ from the experimentally determined energy difference results. The solid red line represents the first ionization threshold of Xe^{3+}, then some states of $4d^{10}5s5p^3nl$ and $4d^{10}5p^4nl$ [$nl = 4f$, $5d$, $6s$ and $6p$], as well as the $4d^95s^25p^4$, $4d^95s5p^5$ and $4d^95s^25p^35d$ autoionizing states, which can decay further into Xe^{4+}. On the other hand, the most important cascade DA inter-

mediate state is $Xe^{2+}4d^95s^25p^5$. The absolute rates for the fine-structure levels of $4d^{10}5s^25p^3$ with red verticals are shown in Fig. 5, along with our electron spectra, convolved with a Gaussian profile of 1.5 eV FWHM for the most important channel Xe^+ $(4p_{3/2}^{-1}) \rightarrow Xe^{2+}4d^95s^25p^5 \rightarrow Xe^{3+}4d^{10}5s^25p^3$, which is in agreement with the experimental spectra,[19] indicating the reliability of our multiple-step approach.

The DA spectra shown in Fig. 4 signify that the autoionization states of Xe^{3+} can decay further via SA decay, leading to cascade TA decay, as described by Eq. (3). Our TA spectra, convolved with a Gaussian profile of 1.5 eV FWHM, are presented in Fig. 6, and are consistent with the experimental measurements.[19] It is found that the initial state Xe^+ $(4p_{3/2}^{-1})$ decays preferentially into the final states $4d^{10}5s^25p^2$; the next and third most populated states are $4d^{10}5s5p^3$ and $4d^{10}5s^25p5d$, respectively. It is also noted that the experimental intensities of the Auger electron spectra could be affected by the background of the coincidences, particularly with regard to the kinetic energy of three Auger electrons at less than 35 eV.

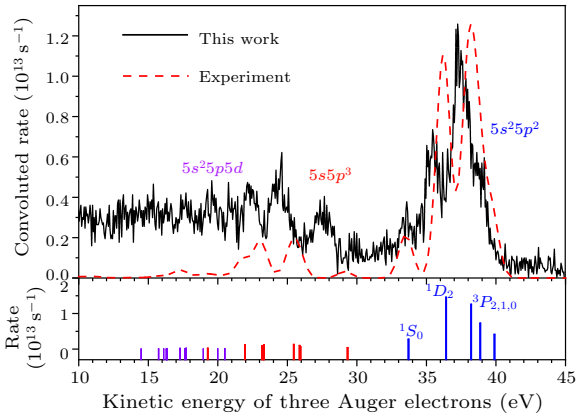

Fig. 6. Theoretical and experimental[19] triple Auger spectra for Xe^+ $(4p_{3/2}^{-1})$ decay. The histogram with colors corresponds to different final-state transition rates.

Table 2. Ion yield ratios (%) of Xe^+ $(4p_{3/2}^{-1})$ together with other theoretical and experimental values produced by single (SA), double (DA), and triple Auger (TA) decay, respectively.

Xe^+ $(4p_{3/2}^{-1})$	This work	Theory[24]	Experiment		
			Ref. [19]	Ref. [22]	Ref. [6]
SA	4.6	3.6	5.0		3.0 ± 1.5
DA	87.0	91.3	86.0	66.0 ± 5.0	62.0 ± 3.0
TA	8.4	5.1	9.0	34.0 ± 5.0	35.0 ± 7.0

Next, we investigate the ion yields produced by SA, DA and TA decay in Xe^+ $(4p_{3/2}^{-1})$. As far as we know, the first results of the ion yield ratios of Xe^+ $(4p_{3/2}^{-1})$ (Xe^{2+}:Xe^{3+}:Xe^{4+} = 3.5 : 91.3 : 5.1) were calculated by Kochur *et al.*[24] in 1994. Later, Hayaishi *et al.*[22] observed complete ion yield ratios ($0 : 66.0 \pm 5.0 : 34.0 \pm 5.0$) using threshold electron-ion coincidence spectroscopy. The most detailed experimental measurements were achieved by Hikosaka *et al.*;[19] these not only provided the ion yield ratios (5.0 : 86.0 : 9.0), but also the Auger spectra, utilizing the efficient multielectron coincidence method. Eland *et al.*,[6] in the most recent experiment using multi-electron multi-ion coincidence methods, determined an ion yield ratio ($3.0 \pm 1.5 : 62.0 \pm 3.0 : 35.0 \pm 7.0$) which is roughly consistent with that of Hayaishi *et al.*,[22] but disagree with the observation of Hikosaka *et al.*[19] as well as the theoretical calculation of Kochur *et al.*[24] We summarize these results, along with ours, in Table 2. Our results (4.6 : 87.0 : 8.4) are extremely close to Hikosaka's experimental results (5.0: 86.0 : 9.0),[19] and better than the previously recorded theoretical results (3.6 : 91.3 : 5.1).[24]

In terms of SA decay, our Xe^{2+} ion yield ratio of 4.6% is consistent with the theoretical value of 3.6%[24] and the experimental values of 5.0%[19] and 3.0%.[6] The ion yield of 87.0% for the cascade DA shown in this work is also close to the preciously reported theoretical and experimental values of 91.3%[24] and 86.0%,[19] respectively. As for TA decay, our production of Xe^{4+} is based on cascade multi-step SA decay. In this approach, the contribution to Xe^{4+} comes from two decay pathways:

(1) Xe^+ $(4p_{3/2}^{-1}) \rightarrow Xe^{2+}4d^95s^25p^4nl$ [nl = $4f$, $6p$, $5d$ and $6s$] $\rightarrow Xe^{3+}$ (mainly $4d^{10}5s5p^35d$ and $4d^{10}5p^45d$) $\rightarrow Xe^{4+}$;

(2) Xe^+ $(4p_{3/2}^{-1}) \rightarrow Xe^{2+}$ (states above the level of $4d^95s^25p^4$) $\rightarrow Xe^{3+}(4d^95s^25p^4$, $4d^95s5p^5$ and $4d^95s^25p^35d) \rightarrow Xe^{4+}$.

The former and latter channels contribute to ion yields of 4.0% and 4.4% for the TA decay, which are reasonably consistent with the experimental findings of 3.0% and 6.0%, respectively.[19] Thus, the contributions of these two channels result in total ion yields of 8.4%, which agrees well with an experimental value of 9.0%.[19] However, a distinct discrepancy in terms of the ion yield ratio remains, meriting further, more detailed experimental investigations.

In conclusion, we have presented detailed theoretical studies of the SA, DA and TA decay of Xe^+ $(4p_{3/2}^{-1})$, in which weak direct processes are neglected, while the dominant cascade processes are included in our calculations. The cascade processes are described via a multi-step process, in which the first

step Auger decay creates an intermediate autoionizing state, embedded energetically within the continuum of the next-higher-charge state, which then decays by means of further electron emission. Large-scale MCDF calculations have been carried out to incorporate the major correlation contributions in successive generations of the initial, intermediate, and final states of the cascade processes. Level-to-level rates for SA, DA and TA decay were obtained for Xe^+ $(4p_{3/2}^{-1})$, with which we were then able to present the corresponding Auger electron spectra and ion yields. Our results show that the Auger electron spectra and ion yields shown in this work are in good agreement with the experimental findings obtained via the multielectron coincidence method.[19] However, it is noted that previously measured ion yields by Eland *et al.*[6] and Hayaishi *et al.*[22] show a distinct difference from the experimental results obtained by Hikosaka *et al.*[19] as well as from ours and previous calculations.[24] Moreover, considering the complexity of the electronic structure of Xe, we also anticipate further, more detailed experiments to explain this unexpected difference.

We would like to thank Professor Yasumasa Hikosaka for providing the experimental data in Ref. [19].

References

[1] Becker U, Szostak D, Kerkhoff H G, Kupsch M, Langer B, Wehlitz R, Yagishita A and Hayaishi T 1989 *Phys. Rev. A* **39** 3902

[2] Penent F, Palaudoux J, Lablanquie P, Andric L, Feifel R and Eland J H D 2005 *Phys. Rev. Lett.* **95** 083002

[3] Gottwald A, Gerth C and Richter M 1999 *Phys. Rev. Lett.* **82** 2068

[4] Carlson T A and Krause M O 1965 *Phys. Rev. Lett.* **14** 390

[5] Muller A, Borovik A, J, Buhr T, Hellhund J, Holste K, Kilcoyne A L, Klumpp S, Martins M, Ricz S, Viefhaus J and Schippers S 2015 *Phys. Rev. Lett.* **114** 013002

[6] Eland J H D, Slater C, Zagorodskikh S, Singh R, Andersson J, Hult-Roos A, Lauer A, Squibb R J and Feifel R 2015 *J. Phys. B* **48** 205001

[7] Hikosaka Y, Lablanquie P, Penent F, Kaneyasu T, Shigemasa E, Eland J H, Aoto T and Ito K 2007 *Phys. Rev. Lett.* **98** 183002

[8] Amusia M Y, Lee I S and Kilin V A 1992 *Phys. Rev. A* **45** 4576

[9] Liu L, Li Y, Gao C and Zeng J 2020 *Phys. Rev. A* **101** 012507

[10] Stock S, Beerwerth R and Fritzsche S 2017 *Phys. Rev. A* **95** 053407

[11] Viefhaus J, Cvejanovic S, Langer B, Lischke T, Prumper G, Rolles D, Golovin A V, Grum-Grzhimailo A N, Kabachnik N M and Becker U 2004 *Phys. Rev. Lett.* **92** 083001

[12] Zhou F, Ma Y and Qu Y 2016 *Phys. Rev. A* **93** 060501

[13] Ma Y, Liu Z, Zhou F and Qu Y 2018 *Phys. Rev. A* **98** 043417

[14] Ma Y, Zhou F, Liu L and Qu Y 2017 *Phys. Rev. A* **96** 042504

[15] Zeng J, Liu P, Xiang W and Yuan J 2013 *Phys. Rev. A* **87** 033419

[16] Wendin G and Ohno M 1976 *Phys. Scr.* **14** 148

[17] Kivima¨K A, Aksela H, Jauhiainen J, Kivilompolo M, Nõmmiste E and Aksela S 1998 *J. Electron Spectrosc. Relat. Phenom.* **93** 89

[18] Heinäsmäki S, Aksela H, Nikkinen J, Kukk E, Kivimäki A, Aksela S and Fritzsche S 2004 *J. Electron Spectrosc. Relat. Phenom.* **137** 281

[19] Hikosaka Y, Lablanquie P, Penent F, Kaneyasu T, Shigemasa E, Eland J H D, Aoto T and Ito K 2007 *Phys. Rev. A* **76** 032708

[20] Ohno M 1995 *J. Electron Spectrosc. Relat. Phenom.* **71** 25

[21] Ohno M 2003 *J. Electron Spectrosc. Relat. Phenom.* **130** 19

[22] Hayaishi T, Matsui T, Yoshii H, Higurash1 A, Murakami E, Yagishita A, Aoto T, Onuma T and Morioka Y 2002 *J. Phys. B* **35** 141

[23] Partanen L, Huttula M, Heinäsmäki S, Aksela H and Aksela S 2007 *J. Phys. B* **40** 4605

[24] Kochur A G, Dudenko A I, Sukhorukov V L and Petrov I D 1994 *J. Phys. B* **27** 1709

[25] Bambynek W, Crasemann B, Fink R W, Freund H U, Mark H and Swift C D 1972 *Rev. Mod. Phys.* **44** 716

[26] Müller A, Borovik A, Buhr T, Hellhund J, Holste K, Kilcoyne A L D, Klumpp S, Martins M, Ricz S, Viefhaus J and Schippers S 2018 *Phys. Rev. A* **97** 013409

[27] Gu M F 2008 *Can. J. Phys.* **86** 675

[28] Ding X B, Dong C Z and Fritzsche S 2008 *Chin. Phys. B* **17** 2033

[29] Fritzsche S 2012 *Comput. Phys. Commun.* **183** 1525

[30] Fischer C F, Gaigalas G, Jönsson P and Bieroń J 2019 *Comput. Phys. Commun.* **237** 184

[31] Jönsson P, He X, Fischer C F and Grant I P 2007 *Comput. Phys. Commun.* **177** 597

[32] Wang X L, Dong C Z, Su M G and Koike F 2012 *Chin. Phys. Lett.* **29** 043201

[33] Ding X B, Dong C Z and O'Sullivan G 2012 *Chin. Phys. Lett.* **29** 063201

[34] Fritzsche S, Fricke B and Sepp W 1992 *Phys. Rev. A* **45** 1465

[35] Fritzsche S, Nikkinen J, Huttula S M, Aksela H, Huttula M and Aksela S 2007 *Phys. Rev. A* **75** 012501

[36] Ma Y, Zhou F, Liu Z and Qu Y 2018 *Chin. Phys. B* **27** 063201